Proceedings of the 21st ICSMGE, Vienna, Austria, 14 – 19 June 2026. Pistrol, Adam & Schweiger (eds.)
Published by: ÖGG, Austrian Society for Geomechanics, Salzburg, Austria, ISBN 978-3-9503898-4-5
https://doi.org/10.53243/ICSMGE2026-1831

Alternative method of pipe roof umbrella design using a simplified numerical model

Sebastjan Kuder, Jure Klopčič, Boštjan Pulko, Janko Logar
University of Ljubljana Faculty of Civil and Geodetic Engineering, Slovenia; sebastjan.kuder@fgg.uni-lj.si

ABSTRACT: When tunneling in a soft ground, the pipe roof umbrella is often being used to improve the stability and safety conditions around the tunnel face. During a tunnel construction, geological conditions often change which requires a modification of the tunnel support parameters. The most optimal way to derive the new parameters is to re-run the numerical analysis. However, when using a pipe roof umbrella system this task can be particularly challenging and requires the use of a 3D computational model due to the complex geometry of the tunnel. Namely, the pipe roof elements fan out along the tunnel axis and the primary lining also follows this contour. Due to the complex 3D shape, the tunnel designer tools incorporated in commercial 3D softwares usually become inadequate, resulting in relatively demanding and time-consuming process of setting up the computational model. This paper presents a theoretical framework of a novel pipe roof umbrella design method, in which the results of a simple numerical analysis utilizing extruded tunnel geometry are combined with the modified semi-analyical displacement function. This novel design method is validated through the results of a complex and precise numerical model, including a parametric study, confirming that the proposed method is effective for various ground conditions.

KEYWORDS: Tunnel, pipe roof, displacement function, 3D analysis.

1 INTRODUCTION

Pipe roof umbrella is one of the pre-support methods in tunneling utilized for an improvement of stability and safety conditions around the unsupported section of the tunnel. For safe but also cost-efficient design of pipe roof umbrella it is necessary to understand the behavior of the pipes during the excavation. Several analytical methods are available for the design of pipe roof, but none has achieved widespread acceptance (Oke et al., 2016).

An empirical displacement function proposed by Barlow (1986) and further modified by Sellner (2000) describes the tunnel displacements as a function of time and excavation advancement. The method has proven to give very good results describing the tunnel displacements, however it has some limitations with regard to describing the pipe roof displacements. Kuder et al. (2024) proposed a modification of the method to overcome these shortcomings. The paper presents results of further research and modification of the existing model to allow for a considerable simplification of the design process.

2 MOTIVATION

In the study presented by Kuder et al. (2022, 2024) the behavior of the pipe roof was analyzed by using a sophisticated and complex 3D numerical model. These analyses confirmed that the pipe roof as a system plays a rather important role in local mechanisms around the tunnel face, but has a very limited overall effect on the tunnel support system.

Since setting up a 3D numerical model with a realistic complex geometry is very labor- and time-consuming and as such rather inappropriate for a day-to-day design work, an idea arose to derive a new method allowing utilization of a simple geometry generated by the integrated software tools and coupled with the abovementioned displacement function. Based on the findings of our previous studies, the pipes could be completely omitted from the simplified model without compromising the credibility of the results in terms of an overall tunnel behavior. Such an approach has the following advantages:

- very simple numerical model obtained by extrusion of the tunnel cross section,
- better defined finite element mesh without very small elements,
- simplified and routine generation of the excavation sequences,
- simplified analyses of results and comparison between the different cases,
- reduced probability for user errors,
- faster calculation and shorter post-processing time.

3 NUMERICAL ANALYSES

Two comparable sets of numerical models were set up, one with complex geometry (Figure 1) and the other with simplified geometry (Figure 2). Both were analyzed with Plaxis 3D program using the same material properties.

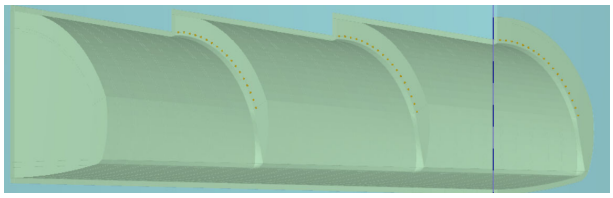

Figure 1. Complex 3D model of the top heading with a temporary invert.

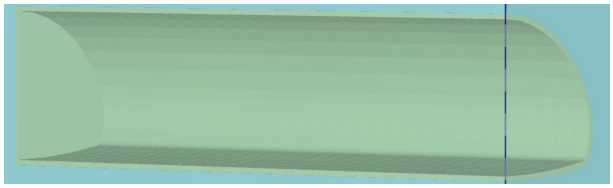

Figure 2. Simplified 3D model of the top heading with a temporary invert.

In the case of a complex numerical model, the pipe elements were modelled as 15 m long beams at 6° inclination, overlapping 5 m along the tunnel axis. Excavation consisted of three 10-meter-long tunnel sections with pipe roof, placed in a model with length 60 m, width 40 m and height 75 m. The pipes were spread in a fan-like pattern with the tunnel lining being aligned with the pipes' contour forming a saw-tooth profile (see Fig. 1).

In the case of a simplified model, the tunnel cross section was simply extruded along the tunnel axis, forming a continuous 30 meters long tunnel tube. Tunnel surface area was 10% enlarged comparing to the average area of the complex model.

As already mentioned, pipe elements were not modelled in the simplified model. Instead, it was presumed that the pipe displacements are essentially the same as the ground displacements at the pipe location.

25 cm thick shotcrete lining was applied at the perimeter and 13 cm for the face stabilization in both cases. Furthermore, the same excavation sequence was modelled in both cases with a typical excavation step of 1 m. For the staged construction, each excavation step was initially excavated with 40% stress relaxation considered, after which the shotcrete layer was activated in the subsequent stage. Since the shotcrete was modelled by an advanced concrete material model, both substages together lasted for 12 hours to account for the shotcrete curing process and its contribution to the evolving displacements.

It has to be noted that in the performed analyses the drained ground conditions were assumed i.e. without presence of ground water. Furthermore, only the top heading was excavated being supported by the temporary invert.

All results shown in this paper are for the pipe at the tunnel crown. Results for the simplified model are recorded at the same location in the tunnel crown as pipes in the complex model using the corresponding line cross sections.

3.1 *Results of the model comparison*

Figure 3 shows vertical displacement curves for two consecutive excavation steps with the excavation face position at -1 m and 0 m in the model. Both dashed curves represent actual pipes in the model with a complex geometry, while other two continuous curves depict the displacements of the model with a simplified geometry.

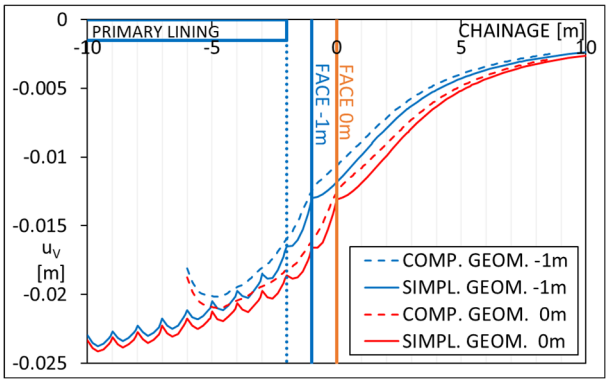

Figure 3. Vertical displacements for the complex and simplified geometry at face position 0 m and -1 m (overburden of 55 m).

Curves of both models match very well approximately 5 m ahead of the face, then separate slightly approaching the face and differ considerably in the unsupported and supported section (supported section is the section of a tunnel where the primary lining was already installed, unsupported section is the excavation step that had just been excavated, but not yet supported). The shape of two curves from the simplified geometry case is much more undulating due to the absence of pipe roof (locally increased deformation in the unsupported section). These curves are shown for an overburden of 55 m, however, the same behavior was observed in all models analyzed at this stage of the study.

One of displacement method modifications proposed by Kuder et al. (2024) is to consider the displacement increments between the two excavation steps rather than the total displacement curves. This requires subtracting two related curves in Fig. 3 for both cases to obtain the curves shown in Fig. 4.

Again, the curves match very well few meters ahead of the face. Surprisingly they match very well also in the supported section, which would not be expected given the shape of the original source curves.

As demonstrated in previous studies, the comparison between the two curves also confirms that the pipe roof affects considerably only the ground behavior around the tunnel face, while having very limited influence to the already excavated and supported tunnel.

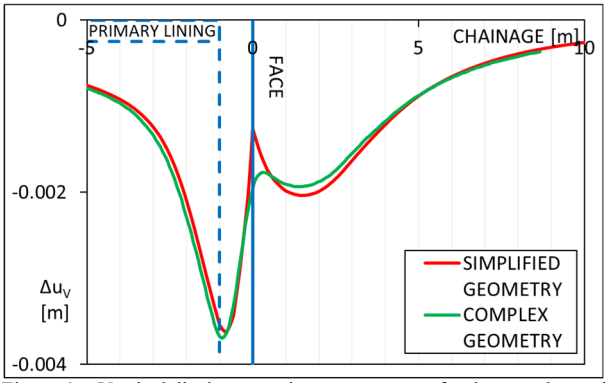

Figure 4. Vertical displacement increment curves for the complex and simple geometry for 55 m overburden.

At the tunnel face, the ground above the newly excavated step is temporarily supported only by the pipe roof and at this stage pipes transfer part of the ground load to the ground ahead of the face and to the supported section of the tunnel. This load transfer results in a substantially larger displacement at the face in the case of a complex geometry model. As can be seen from Fig. 4, vertical displacements are slightly reduced few meters ahead of the face due to the pipe roof effect.

Furthermore, the incremental displacement curves were compared across several additional cases with varying input parameters. Figure 5 shows comparison of curves for the low overburden case (15 m).

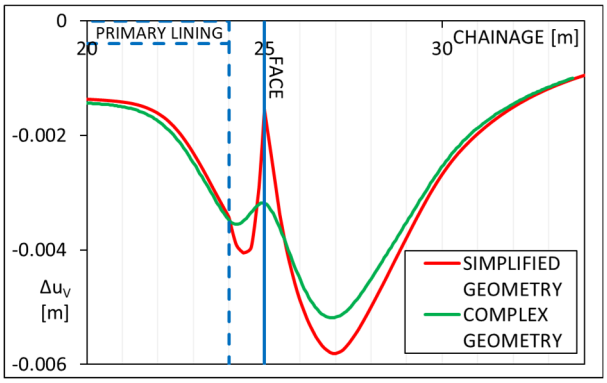

Figure 5. Vertical displacement increment curves for the complex and simplified geometry for 15 m overburden and softer ground.

Curves for the low overburden in Fig. 5 and curves for the high overburden in Fig. 4 have some similar patterns (e.g. at the face) but also have some clearly different properties. In Fig. 5 the displacements few meters ahead of the face are considerably higher than in the unsupported section comparing to Fig. 4, likely due to the lower strength and stiffness properties of the ground. The displacements of a simplified model (i.e. without the pipe roof) are considerably larger in the unsupported section and few meters ahead of the face than in the case of a complex model. This behavior is considerably more pronounced in case of the lower overburden in Fig. 5 when compared to Fig.4, again due to lower strength and stiffness ground properties.

Cases presented in Figs. 4 and 5 show two border scenarios. Across the study, response patterns were obtained that mostly resemble either of the two or anywhere in-between. Furthermore, the results showed that in addition to the stiffness and strength properties of the ground, the response patterns can also be influenced by variations in the primary lining stiffness and the initial stress state (Kuder et al. 2022).

Importantly, both displacement curves match very well in the supported section as well as in the section ahead of the face for both border cases shown in Figs. 4 and 5. Since Kuder et al. (2024) showed on models with a complex geometry that these two outer sections can be effectively described by using the displacement function method, this important observation further supports our initial assumption that the same approach can be applied to the simplified geometry models.

4 DISPLACEMENT FUNCTION METHOD

Originally, Barlow (1986) proposed three separate functions to describe the tunnel crown displacement. The first function describes the displacements ahead of the face in an unexcavated ground (1), the second in the unsupported section (2) and the third in the supported section (3) as shown in Fig. 6. Further modifications were introduced by Sellner (2000).

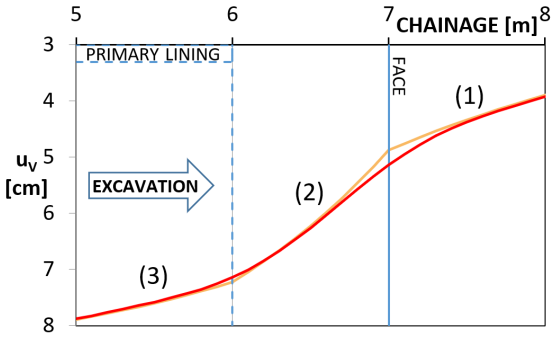

Figure 6. Three displacement functions (brown curve) and numerically obtained displacement curve (red).

In general, the theoretical displacement functions align closely with the numerically obtained curve. However, there are discrepancies particularly around the point of contacts between the three functions, where considerable differences between displacements and inclinations are observed. It is obvious, that such displacement functions (especially the intermediate function) do not represent the actual response of a material point due to the tunnel excavation well enough to be reliably used for the assessment of pipe roof internal forces based on the ground displacement.

To overcome these deficiencies, Kuder et al. (2024) proposed a semi-analytical model by replacing the intermediate displacement function with a series of uniform and triangular loads acting on the beam being partly supported by the elastic Winkler subspace (Fig. 7). The beam was assigned the same displacements at both ends as calculated with the original displacement functions to have the appropriate boundary conditions.

The modified model was further on calibrated to the curves obtained by a series of numerical analyses on the complex geometry models. However, this modified model tended to be less appropriate for the simplified geometry which yields different curves as shown previously, therefore an additional modification was required.

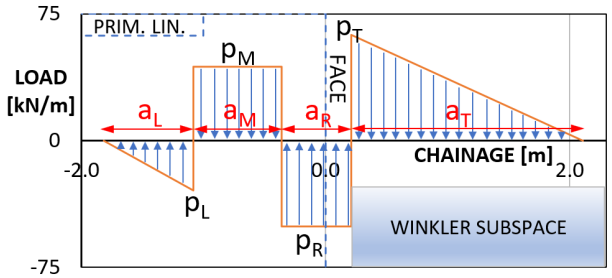

Figure 7. Proposed analytical solution for the intermediate section of the pipe roof (Kuder et al., 2024).

5 MODIFIED SEMI-ANALYTICAL MODEL OF THE PIPE ROOF ELEMENT

One of the disadvantages of the proposed semi-analytical model was a relatively high number of variables to be determined within the fitting procedure. To address this, a further modification was introduced to reduce the number of variables. Namely, in the previous model, the section length values a_L, a_M, a_R, a_T and load size values p_L, p_M, p_R, p_T were all determined by the best fit method. In the new model, only the a_T value is determined by fitting, while the other three section lengths are now defined by the model geometry. Specifically, the section length a_R is defined by the thickness of the face shotcrete t_F, increased on both ends by a half of the lining thickness t_L

$$a_R = t_F + t_L \,. \tag{1}$$

The p_R load thus reaches a half of the lining thickness into the ground ahead of the face (Fig. 8). This pattern was regularly observed in the previous analyses. The section length a_M extends from the tunnel side of section a_R to the edge of the primary lining

$$a_M = L_R - a_R + t_L/2 \,, \tag{2}$$

where L_R equals the excavation round length. The section length of the triangular load a_L also equals the round length.

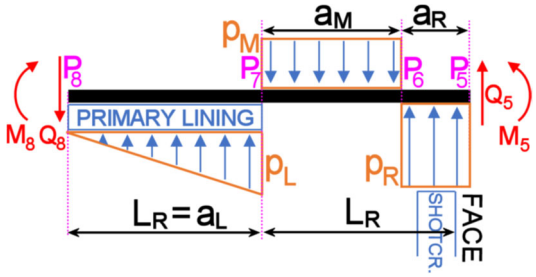

Figure 8. Newly defined intermediate load distribution in the unsupported and supported sections.

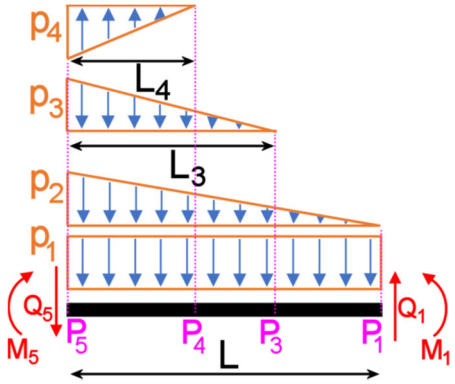

Figure 9. Newly defined intermediate load distribution ahead of the face.

The second modification was aimed at redefining the intermediate functions ahead of the face, which are based on the Winkler subgrade model. The newly defined model retains the analytical approach for a beam on an elastic support by Young and Budynas (2002), but adopts solutions for the finite length beam instead of a semi-infinite beam. Although this modification introduces two new triangular loads (loads p_1 and p_2 in Fig. 9), it greatly simplifies the conditions at the contact, where the boundary conditions are defined by the original displacement function. Namely, a triangular or uniform load extending across the entire beam causes an elastically supported beam to move as a rigid body, while not affecting the bending moments. Therefore, the purpose of loads p_1 and p_2 is solely to meet the displacement and rotation conditions at the contact. A relatively small moment M_1 and vertical force Q_1 are added to meet the boundary conditions and since the pipe is relatively long and flexible these boundary conditions at the contact are automatically fulfilled, regardless if any of the model parameters (e.g. loads, subgrade reaction modulus, etc.) change. The position of point P_1 is set by hand and corresponds roughly to the height of the excavation. In general, matching of the displacement and numerical curves is very good and therefore the position of the point P_1 does not have to be very accurate. In any case, it should be outside of the area of significant plastic deformations.

The purpose of the triangular load p_3 is to adjust the curve at the point P_3 where the slope of numerically obtained curve becomes steeper. Both p_3 and P_3 are easily determined by hand. However, the p_3 value needs to be adjusted each time the subgrade reaction modulus changes.

The triangular load p_4 normally acts upwards. Its purpose is to form the inflection point to align with the numerically obtained curve which often has trench-like shape at this section. The p_4 value is crucial for the correct curve shape at the face and is one of four variables to be determined by the computer solver. The position of point P_4 is not very important for the final solution and is determined by hand. By moving the P_4 position and changing the subgrade reaction modulus at the same time, a very good agreement with the numerically obtained curve can be obtained. However, this has a very little impact on the overall results as it will be discussed later. In some special instances, when the p_R load is dominant the p_3 load can act downwards.

The following additional assumptions apply to the model:

- two original displacement functions describe the pipe behavior at both ends. Their parameters are determined by fitting the shapes of both functions to the numerically obtained curves,
- the pipe element is modelled as linear elastic beam with known relations between displacements and internal forces,
- four boundary conditions (displacement, rotation, bending moment, shear force) are met at each contact between two adjacent displacement functions,
- the derivatives and resulting internal forces are obtained analytically.

5.1 *Numerical solution of the system*

As noted above, many function parameters are determined either numerically or by hand using the best fit method. Their values do not affect the final results as long as the derived functions appropriately fit to the numerically obtained curve at particular sections. However, there are four main unknown parameters that need to be determined in order to acquire the correct bending moment curve which is the final goal of the proposed design method. These variables are p_L, p_M, p_R and p_4 (Figs. 8 and 9) which can be derived using the computer solver. In order to solve the system, four conditions shall be met. As already mentioned, the boundary conditions at point P_1 (the contact between the beam and the displacement function ahead of the face) are met automatically and they do not influence the rest of the system.

Thus, four conditions at the point P_8 (Fig. 8) shall be met: equality of vertical displacement u_{z1}, rotation ω_1, bending moment M_1 and shear force Q_1, all defined by the displacement function in the supported section. To find the solution, the beam is separated at the contact and the known values M_8 and Q_8 become the joint load at the right side (Fig. 8). Therefore, only two conditions need to be met at this joint: u_{z8} and ω_8. The first remaining condition is the value of the displacement increment u_z at the face – the "spike" in Figs. 4 and 5. Due to the spike, the resulting bending moment at this point will be higher than the numerical one. In terms of the design process this means that the final result will be on the safe side. The last remaining condition was derived based on the observation that the local minimum bending moment increment is always at the face or at least very close to it. This means that the corresponding shear force has to be zero at this point. This is the fourth and the final condition that has to be set in the computer solver in order to determine the four unknown loads.

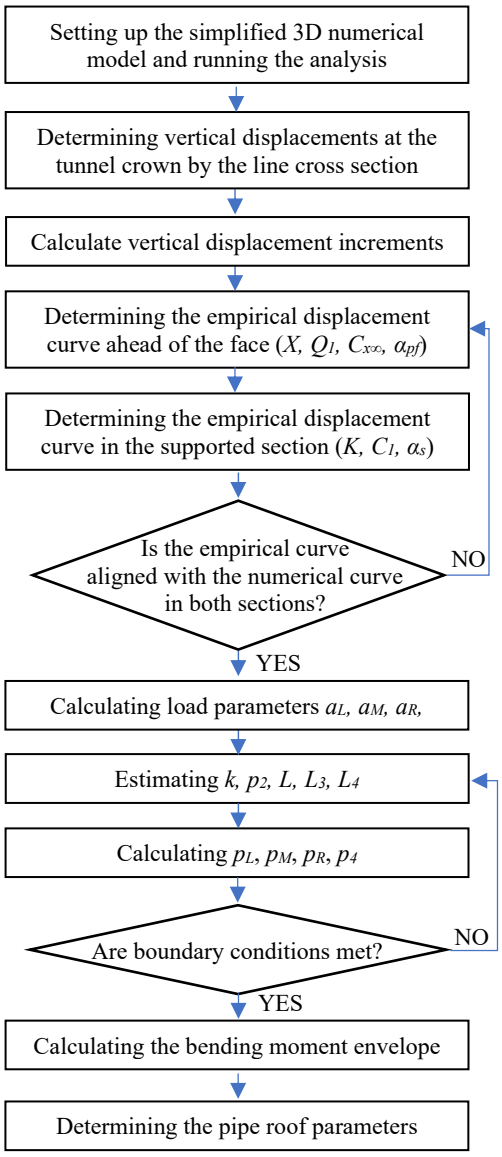

Figure 10. Flow chart of the design method.

Once the boundary conditions are met and the shape of the displacement curve is satisfactory, the total bending moment envelope can be calculated by adding together a series of consecutive increments.

As it is shown in Figure 10, the process of finding the solution is relatively straightforward, requiring only few interventions by the engineer.

6 THEORETICAL BACKGROUND

6.1 *Original displacement functions*

At both ends of the proposed model the pipe displacements are described by original displacement functions by Barlow (1986) and Sellner (2000). Equation (3) describes displacement ahead of the face and Equation (4) in supported section:

$$C_{pf}(x,t) = \left[Q_1 \cdot \left[\frac{X}{X+(x_f-x)}\right]^{\alpha_{pf}} - Q_k \cdot P_k^+(x)\right] \cdot [C_{x\infty} + A \cdot C_2(t)] \quad (3)$$

$$C_s(x,t) = [Q_1 + Q_2 \cdot C_1(x) + K \cdot C_s - Q_k \cdot P_k^-(x)] \cdot \frac{[C_{x\infty} + A \cdot C_2(t)]}{[1 + K \cdot (C_{x\infty} + A \cdot C_2(t))]} \quad (4)$$

Auxiliary function $C_1(x)$ is defined as

$$C_1(x) = \left[1 - \frac{X}{X+x}\right]^{\alpha_s} \quad (5)$$

Here Q_1 is a displacement proportion ahead of the face, X, α_{pf} and α_s are empirical parameters, Q_k is a displacement proportion to account for the effect of support, P_k^+ is a support function ahead of the support installation point, $C_{x\infty}$ is the time independent displacement, A is a displacement proportion to account for the effect of time, C_2 is a displacement function to account for the time effect, Q_2 is a displacement proportion in the supported section, C_s is a displacement function in the supported section, P_k^- is a support function behind the support installation point, K is a support stiffness and C_S is the convergence at the point of support installation.

Originally, the four main parameters ($C_{x\infty}$, Q_1, A and X) are determined by the fitting process. In order to achieve the best fit for several consecutive curves, parameters K, α_{pf} and α_s needed to be fitted as well.

Again, it should be noted that the time dependent ground behaviour was not considered in the numerical analyses (A=0). In addition, in Equations (3), (4) and (5) the coordinate system was reversed so that these expressions describe the displacements along the tunnel length at the certain face position instead of the displacement at the certain cross section as a function of the face position (Kuder et al., 2024).

6.2 *Linear beam on elastic foundation*

For the section ahead of the face, the displacement curve was determined by superimposing the contributions of four distributed loads and four point loads at both ends (Figure 9). With the exception of loads p_3 and p_4, the rest are determined by meeting the boundary conditions.

The beam is supported by an elastic ground. The corresponding solutions by Young and Budynas (2002) for the finite length beam are adopted for each type of the load. Below only a set of equations (6) to (18) for bending moment due to triangular load is displayed (Figure 11). The beam has no displacement or rotation constraints at both ends.

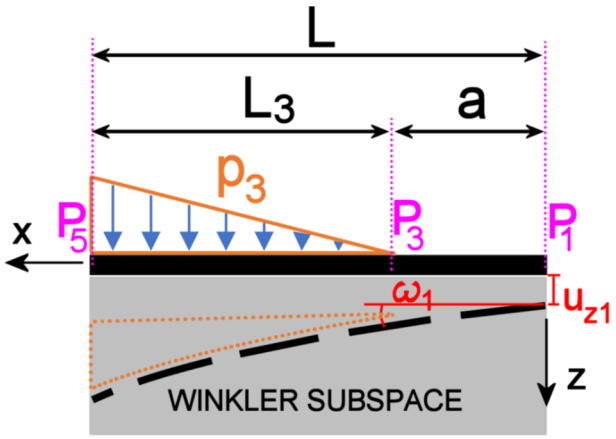

Figure 11. Triangular load on a beam on elastic foundation.

$$M = -2u_{z1}EI\beta^2 F_3 - \omega_1 EI\beta F_4 - \frac{p_3 F_{a4}}{4\beta^3 L_3} \quad (6)$$

$$\beta = \sqrt[4]{bk/(4EI)} \quad (7)$$

$$u_{z1} = \frac{p_3(C_4C_{a3} - C_3C_{a4})}{4EI\beta^5 L_3 C_{11}} \quad (8)$$

$$\omega_1 = \frac{p_3(C_2C_{a4} - C_3C_{a3})}{4EI\beta^4 L_3 C_{11}} \quad (9)$$

$$F_3 = \sinh\beta x \sin\beta x \quad (10)$$

$$F_4 = \cosh\beta x \sin\beta x - \sinh\beta x \cos\beta x \quad (21)$$

$$F_{a4}(x > a) = cosh\,\beta(x-a)\,sin\,\beta(x-a) - \sinh\beta(x-a)\cos\beta(x-a) \quad (32)$$

$$C_2 = \cosh\beta L \sin\beta L + \sinh\beta L \cos\beta L \quad (43)$$

$$C_3 = \sinh\beta L \sin\beta L \quad (54)$$

$$C_4 = \cosh\beta L \sin\beta L - \sinh\beta L \cos\beta L \quad (65)$$

$$C_{11} = \sinh^2\beta L - \sin^2\beta L \quad (76)$$

$$C_{a3} = \sinh\beta L_3 \sin\beta L_3 \quad (87)$$

$$C_{a4} = \cosh\beta L_3 \sin\beta L_3 - \sinh\beta L_3 \cos\beta L_3 \quad (98)$$

Parameter b is axial distance between pipes.

7 PRACTICAL EXAMPLE

As an example, the results of the top heading excavation are presented. Table 1 displays the input parameters for the complex and simplified geometry alike.

Table 2 displays the resulting displacement function properties and loads acting on the beam obtained by fitting the curves and subsequent solving of the system.

The curves in Figure 12 and values in Table 2 allow for a direct comparison between the numerical and semi-analytical approaches. The displacement curve of a simplified numerical model matches well with the curve obtained by the proposed semi-analytical model. On the other hand, the bending moment curve of the proposed semi-analytical model have considerably higher extreme values than the curve obtained with the complex numerical model. As shown in the lowest rows of Table 2, the difference for the minimal value is 68% and for maximal value is 46%. In terms of the design process, the safety factor of the proposed semi-analytical method can be estimated as 1.7.

Table 1. Main properties of the numerical model.

Parameter	Value	Unit
Average top heading radius	approx. 6	m
Overburden height	55	m
Lining shotcrete thickness	25	cm
Face shotcrete thickness	13	cm
Ground angle of internal friction	28	°
Ground cohesion	35	kPa
Ground modulus $E_{50} = E_{oed}$	100	MPa
Pipe diameter	114	mm
Pipe bending stiffness	655	kNm^2

Table 2. Results for the proposed semi-analytical model.

Parameter	Value	Unit
$C_{x\infty}$	11.88	cm
Q_1	0.25	-
K	61.8	m^{-1}
X	2.32	m
α_{pf}	1.39	-
α_s	1.16	-
Subgrade modulus	190	MN/m^3
Load p_L	-37.9	kN/m
Load p_M	82.1	kN/m
Load p_R	-120.5	kN/m
Load p_3	72.0	kN/m
Load p_4	-99.5	kN/m
x_{P4}	1.6	m
x_{P3}	4.5	m
x_{P1}	6.0	m
Minimal bending moment (difference)	-6.18 (68%)	kNm
Maximal bending moment (difference)	6.32 (46%)	kNm

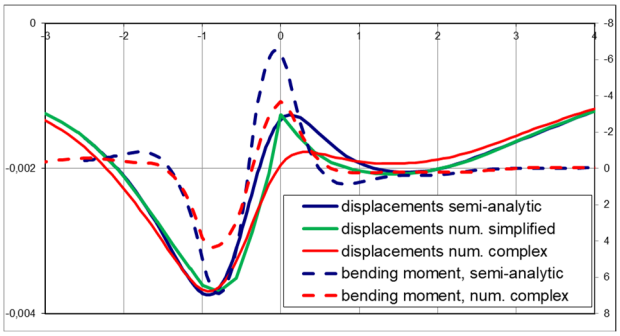

Figure 12. Comparison of the displacement and bending moment curves.

8 PARAMETRIC STUDY - VARIATION OF SUBGRADE REACTION MODULUS

Within the analysis, another parametric study was conducted varying the value of subgrade reaction modulus. Initially, the value was estimated based on the ground elastic modulus, tunnel geometry and pipe properties. Obtained value (190 MN/m^3) served as a reference value. Based on the results shown in Table 3, it can be concluded that varying the modulus greatly affects the calculated loads p_3 and p_4, but has a very limited effect on the bending moments within the pipe, which confirms the generally accepted assumption regarding the behavior of the beam on the elastic foundation.

Table 3. Results of variation of subgrade reaction modulus.

Parameter	Set 1	Set 2	Set 3	Unit
Subgrade modulus k	100	190	400	MN/m^3
Load p_L	-121.0	-120.5	-119.9	kN/m
Load p_4	-38.7	-99.5	-227.0	kN/m
Coordinate x_{P4}	1.6	1.6	1.6	m
Load p_3	35	72	160	kN/m
Bend. mom. M_{max}	6.33	6.32	6.30	kNm
Bend. mom. M_{min}	-6.23	-6.18	-6.13	kNm

9 CONCLUSIONS

Complex 3D numerical analyses are costly and time-consuming approach to analyze the behavior of pipe roof. For this reason, it was assumed and verified that the use of a simplified geometry with a constant cross section and without modelling pipes can provide adequate results. Based on these findings and relying on the existing solutions, a new semi-analytical method is proposed.

The simplified geometry yields on average very similar displacements compared to the complex geometry, but it very distinctly underestimates the displacements at the tunnel face. By considering this boundary condition in the calculations, the resulting bending moments remain conservative but tend to be quite overestimated. Overall, it is estimated that the simplified approach yields safety factor of approximately 1.7 regarding bending moments. The parametric study further demonstrated that moderately inaccurate values of the subgrade reaction modulus can still produce stable and reliable estimates of extreme bending moments.

10 REFERENCES

Barlow, J.P. 1986. Interpretation of Tunnel Convergence Measurements. *Master thesis. University of Alberta, Department of Civil & Environmental Engineering*. Edmonton, Canada.

Kuder, S., Logar, J., and Klopčič, J. 2022. The numerical study of umbrella arch behavior in soft ground tunneling. *Proceedings of the 20th International Conference on Soil Mechanics and Geotechnical Engineering– Rahman and Jaksa (Eds.*), Sydney, 2183-2187.

Kuder, S., Klopčič, J., Pulko, B., and Logar, J. 2024. An advanced method to predict umbrella arch behaviour in soft ground tunnelling. *Proceedings of XVIII European Conference on Soil Mechanics and Geotechnical Engineering*, Lisbon, 596-599.

Oke, J., Vlachopoulos, N., and Diederichs, M.S. 2016. Semi-analytical model for umbrella arch systems employed in squeezing ground conditions, *Tunnelling and Underground Space Technology*, 56. Available at: https://doi.org/10.1016/j.tust.2016.03.006.

Sellner, P.J. 2000. Prediction of Displacements in Tunneling. *Doctoral Thesis. Graz University of Technology, Institute for Rock Mechanics and Tunnelling*, Graz, Austria.

Young, W.C., and Budynas, R.G. 2002. Roark's formulas for Stress and Strain, 7th Edition, McGraw Hill.